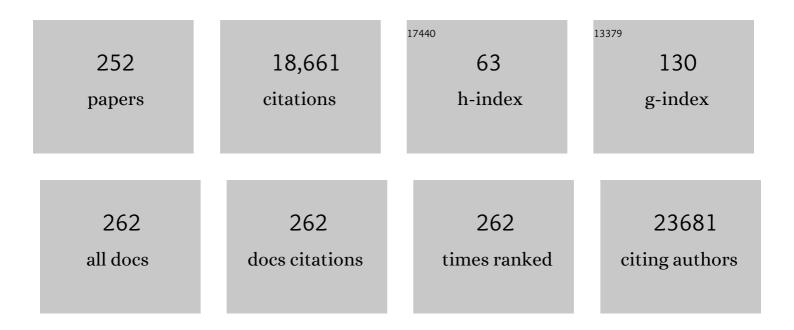
## Jung Ho Kim

List of Publications by Year in descending order

Source: https://exaly.com/author-pdf/9541866/publications.pdf Version: 2024-02-01



LUNC HO KIM

#	Article	IF	CITATIONS
1	Cobalt supported nitrogen-doped carbon nanotube as efficient catalyst for hydrogen evolution reaction and reduction of 4-nitrophenol. Applied Surface Science, 2022, 572, 151450.	6.1	16
2	Interfacial reaction and side effect of MgB2 superconducting material through low-rotation mechanical milling. Ceramics International, 2022, 48, 6539-6548.	4.8	6
3	MgB <sub>2</sub> Superconducting Joint Architecture with the Functionality to Screen External Magnetic Fields for MRI Magnet Applications. ACS Applied Materials & Interfaces, 2022, 14, 3418-3426.	8.0	8
4	7 T Niobium-Titanium-Based Persistent-Mode Superconducting Magnet for an Electron Beam Ion Source. IEEE Access, 2022, 10, 14731-14738.	4.2	0
5	The advent of manganese-substituted sodium vanadium phosphate-based cathodes for sodium-ion batteries and their current progress: a focused review. Journal of Materials Chemistry A, 2022, 10, 1022-1046.	10.3	26
6	Mechanistic and nanoarchitectonics insight into Li–host interactions in carbon hosts for reversible Li metal storage. Nano Energy, 2022, 95, 106999.	16.0	22
7	Intrinsic electrochemical activity of Ni in Ni3Sn4 anode accommodating high capacity and mechanical stability for fast-charging lithium-ion batteries. Journal of Energy Chemistry, 2022, 71, 470-477.	12.9	7
8	Allâ€day wearable health monitoring system. EcoMat, 2022, 4, .	11.9	29
9	Hydrogen evolution reaction catalyst with high catalytic activity by interplay between organic molecules and transition metal dichalcogenide monolayers. Materials Today Energy, 2022, 25, 100976.	4.7	4
10	Porous carbon architectures with different dimensionalities for lithium metal storage. Science and Technology of Advanced Materials, 2022, 23, 169-188.	6.1	21
11	Resistive Water Level Sensors Based on AgNWs/PEDOT:PSS- <i>g</i> -PEGME Hybrid Film for Agricultural Monitoring Systems. ACS Omega, 2022, 7, 15459-15466.	3.5	2
12	Patchable and Implantable 2D Nanogenerator. Small, 2021, 17, e1903519.	10.0	30
13	Superconducting Joining Concept for Internal Magnesium Diffusion-Processed Magnesium Diboride Wires. ACS Applied Materials & Interfaces, 2021, 13, 3349-3357.	8.0	12
14	Suppression of dendritic lithium-metal growth through concentrated dual-salt electrolyte and its accurate prediction. Journal of Materials Chemistry A, 2021, 9, 22833-22841.	10.3	10
15	Solvothermally synthesized anatase TiO2 nanoparticles for photoanodes in dye-sensitized solar cells. Science and Technology of Advanced Materials, 2021, 22, 100-112.	6.1	16
16	2D Nanogenerators: Patchable and Implantable 2D Nanogenerator (Small 9/2021). Small, 2021, 17, 2170039.	10.0	0
17	Evaluation and control of residual amorphous phases in carbon-doped MgB2 superconductors. Journal of Alloys and Compounds, 2021, 864, 158867.	5.5	8
18	Structurally stabilized lithium-metal anode via surface chemistry engineering. Energy Storage Materials, 2021, 37, 315-324.	18.0	46

#	Article	IF	CITATIONS
19	Design of cobalt catalysed carbon nanotubes in bimetallic zeolitic imidazolate frameworks. Applied Surface Science, 2021, 547, 149134.	6.1	33
20	Stabilizing Li-metal host anode with LiF-rich solid electrolyte interphase. Nano Convergence, 2021, 8, 18.	12.1	12
21	Critical role of surface craters for improving the reversibility of Li metal storage in porous carbon frameworks. Nano Energy, 2021, 88, 106243.	16.0	16
22	Superconducting joints using multifilament MgB2 wires for MRI application. Scripta Materialia, 2021, 204, 114156.	5.2	16
23	Nickel-Iron nitrides and alloy heterojunction with amorphous N-doped carbon Shell: High-efficiency synergistic electrocatalysts for oxygen evolution reaction. Applied Surface Science, 2021, 566, 150706.	6.1	22
24	Fundamental insight in the design of multifilament MgB <sub>2</sub> joint for boosting the persistent-mode operation. Superconductor Science and Technology, 2021, 34, 125003.	3.5	5
25	Strategic Approaches to the Dendritic Growth and Interfacial Reaction of Lithium Metal Anode. Chemistry - an Asian Journal, 2021, 16, 4010-4017.	3.3	17
26	Mechanically Stable Kirigami Deformable Resonant Circuits for Wireless Vibration and Pressure Sensor Applications. ACS Applied Materials & Interfaces, 2021, 13, 54162-54169.	8.0	6
27	Enriched Cavities to ZIF-8-Derived Porous Carbon for Reversible Metallic Lithium Storage. ACS Applied Energy Materials, 2021, 4, 14520-14525.	5.1	5
28	Hierarchically open-porous nitrogen-incorporated carbon polyhedrons derived from metal-organic frameworks for improved CDI performance. Chemical Engineering Journal, 2020, 382, 122996.	12.7	84
29	MgB <sub>2</sub> for MRI applications: dual sintering induced performance variations in <i>in situ</i> and IMD processed MgB <sub>2</sub> conductors. Journal of Materials Chemistry C, 2020, 8, 2507-2516.	5.5	21
30	Tailored joint fabrication process derived ultra-low resistance MgB2 superconducting joint. Scripta Materialia, 2020, 178, 198-202.	5.2	15
31	nâ€ZnO/pâ€NiO Core/Shellâ€ <del>S</del> tructured Nanorods for Piezoelectric Nanogenerators. Energy Technology, 2020, 8, 2070103.	3.8	1
32	Interplay between cold densification and malic acid addition (C4H6O5) for the fabrication of near-isotropic MgB2 conductors for magnet application. Journal of Magnesium and Alloys, 2020, 8, 493-498.	11.9	7
33	Focus on nanogenerators: toward smart wearable devices. Science and Technology of Advanced Materials, 2020, 21, 422-423.	6.1	4
34	Lithium metal storage in zeolitic imidazolate framework derived nanoarchitectures. Energy Storage Materials, 2020, 33, 95-107.	18.0	40
35	nâ€ZnO/pâ€NiO Core/Shellâ€Structured Nanorods for Piezoelectric Nanogenerators. Energy Technology, 2020, 8, 2000462.	3.8	2
36	Bottom-Up Lithium Growth Triggered by Interfacial Activity Gradient on Porous Framework for Lithium-Metal Anode. ACS Energy Letters, 2020, 5, 3108-3114.	17.4	102

#	Article	IF	CITATIONS
37	Tailoring Domain Morphology in Monolayer NbSe <sub>2</sub> and W <sub><i>x</i></sub> Nb <sub>1–<i>x</i></sub> Se <sub>2</sub> Heterostructure. ACS Nano, 2020, 14, 8784-8792.	14.6	30
38	Functionality of Dualâ€Phase Lithium Storage in a Porous Carbon Host for Lithiumâ€Metal Anode. Advanced Functional Materials, 2020, 30, 1910538.	14.9	68
39	Morphology adjustable CoxN with 3D mesoporous structure and amorphous N-doped carbon for overall water splitting. Applied Surface Science, 2020, 529, 147177.	6.1	24
40	Biomolecular Piezoelectric Materials: From Amino Acids to Living Tissues. Advanced Materials, 2020, 32, e1906989.	21.0	134
41	Tunable porosity in bimetallic core-shell structured palladium-platinum nanoparticles for electrocatalysts. Scripta Materialia, 2019, 158, 38-41.	5.2	13
42	Everlasting Living and Breathing Gyroid 3D Network in Si@SiOx/C Nanoarchitecture for Lithium Ion Battery. ACS Nano, 2019, 13, 9607-9619.	14.6	165
43	Optical logic operation via plasmon-exciton interconversion in 2D semiconductors. Scientific Reports, 2019, 9, 9164.	3.3	12
44	Design of 2D Nanocrystalline Fe <sub>2</sub> Ni <sub>2</sub> N Coated onto Graphene Nanohybrid Sheets for Efficient Electrocatalytic Oxygen Evolution. ACS Applied Energy Materials, 2019, 2, 8502-8510.	5.1	25
45	Niobium-titanium (Nb-Ti) superconducting joints for persistent-mode operation. Scientific Reports, 2019, 9, 14287.	3.3	24
46	Edge Contact for Carrier Injection and Transport in MoS <sub>2</sub> Field-Effect Transistors. ACS Nano, 2019, 13, 13169-13175.	14.6	47
47	Oxygen-Deficient TiO2-δ Synthesized from MIL-125 Metal-Organic Framework for Photocatalytic Dye Degradation. Bulletin of the Chemical Society of Japan, 2019, 92, 2012-2018.	3.2	7
48	Rationally designed bimetallic Au@Pt nanoparticles for glucose oxidation. Scientific Reports, 2019, 9, 894.	3.3	31
49	Electrochemical properties of nonstoichiometric silicon suboxide anode materials with controlled oxygen concentration. Composites Part B: Engineering, 2019, 174, 107024.	12.0	25
50	Ultra-thin, highly graphitized carbon nanosheets into three-dimensional interconnected framework utilizing a ball mill mixing of precursors. Chemical Engineering Journal, 2019, 374, 1214-1220.	12.7	18
51	In-situ formation of MOF derived mesoporous Co3N/amorphous N-doped carbon nanocubes as an efficient electrocatalytic oxygen evolution reaction. Nano Research, 2019, 12, 1605-1611.	10.4	108
52	Mesoporous carbon cubes derived from fullerene crystals as a high rate performance electrode material for supercapacitors. Journal of Materials Chemistry A, 2019, 7, 12654-12660.	10.3	86
53	A Comparative Study of TiO2 Paste Preparation Methods Using Solvothermally Synthesised Anatase Nanoparticles in Dye-Sensitised Solar Cells. Applied Sciences (Switzerland), 2019, 9, 979.	2.5	3
54	Temperature-dependent piezotronic effect of MoS2 monolayer. Nano Energy, 2019, 58, 811-816.	16.0	26

#	Article	IF	CITATIONS
55	Au decorated core-shell structured Au@Pt for the glucose oxidation reaction. Sensors and Actuators B: Chemical, 2019, 278, 88-96.	7.8	71
56	Cubic aggregates of Zn2SnO4 nanoparticles and their application in dye-sensitized solar cells. Nano Energy, 2019, 57, 202-213.	16.0	42
57	Indium Oxide/Carbon Nanotube/Reduced Graphene Oxide Ternary Nanocomposite with Enhanced Electrochemical Supercapacitance. Bulletin of the Chemical Society of Japan, 2019, 92, 521-528.	3.2	88
58	Piezo/triboelectric nanogenerators based on 2-dimensional layered structure materials. Nano Energy, 2019, 57, 680-691.	16.0	108
59	Si Nanocrystal-Embedded SiO x nanofoils: Two-Dimensional Nanotechnology-Enabled High Performance Li Storage Materials. Scientific Reports, 2018, 8, 6904.	3.3	11
60	Facile Synthesis of Palladiumâ€Nanoparticleâ€Embedded Nâ€Doped Carbon Fibers for Electrochemical Sensing. ChemPlusChem, 2018, 83, 401-406.	2.8	8
61	Efficient wide range electrochemical bisphenol-A sensor by self-supported dendritic platinum nanoparticles on screen-printed carbon electrode. Sensors and Actuators B: Chemical, 2018, 255, 2800-2808.	7.8	63
62	The effect of amorphous TiO <sub>2</sub> in P25 on dye-sensitized solar cell performance. Chemical Communications, 2018, 54, 381-384.	4.1	36
63	Mesoporous Manganese Phosphonate Nanorods as a Prospective Anode for Lithium-Ion Batteries. ACS Applied Materials & Interfaces, 2018, 10, 19739-19745.	8.0	38
64	Strategically Designed Zeolitic Imidazolate Frameworks for Controlling the Degree of Graphitization. Bulletin of the Chemical Society of Japan, 2018, 91, 1474-1480.	3.2	38
65	Evaluation of a solid nitrogen impregnated MgB <sub>2</sub> racetrack coil. Superconductor Science and Technology, 2018, 31, 105010.	3.5	25
66	Superior transport J c obtained in in-situ MgB 2 wires by tailoring the starting materials and using a combined cold high pressure densification and hot isostatic pressure treatment. Scripta Materialia, 2017, 129, 79-83.	5.2	18
67	Theoretically designed metal-welded carbon nanotubes: Extraordinary electronic properties and promoted catalytic performance. Nano Energy, 2017, 32, 209-215.	16.0	17
68	Mesoporous Ni–Fe oxide multi-composite hollow nanocages for efficient electrocatalytic water oxidation reactions. Journal of Materials Chemistry A, 2017, 5, 4320-4324.	10.3	108
69	Nanotechnology and its medical applications: revisiting public policies from a regulatory perspective in Australia. Nanotechnology Reviews, 2017, 6, 255-269.	5.8	8
70	Fish Gill Inspired Crossflow for Efficient and Continuous Collection of Spilled Oil. ACS Nano, 2017, 11, 2477-2485.	14.6	186
71	Synergistic effect of Indium and Gallium co-doping on growth behavior and physical properties of hydrothermally grown ZnO nanorods. Scientific Reports, 2017, 7, 41992.	3.3	50
72	Solid cryogen: a cooling system for future MgB2 MRI magnet. Scientific Reports, 2017, 7, 43444.	3.3	27

#	Article	IF	CITATIONS
73	Highly Ordered Mesostructured Vanadium Phosphonate toward Electrode Materials for Lithiumâ€ion Batteries. Chemistry - A European Journal, 2017, 23, 4344-4352.	3.3	30
74	Hollow carbon nanobubbles: monocrystalline MOF nanobubbles and their pyrolysis. Chemical Science, 2017, 8, 3538-3546.	7.4	329
75	Research Update: Hybrid energy devices combining nanogenerators and energy storage systems for self-charging capability. APL Materials, 2017, 5, .	5.1	59
76	Understanding chemically processed solar cells based on quantum dots. Science and Technology of Advanced Materials, 2017, 18, 334-350.	6.1	32
77	Synthesis and Cytotoxicity of Dendritic Platinum Nanoparticles with HEKâ€293 Cells. Chemistry - an Asian Journal, 2017, 12, 21-26.	3.3	25
78	Threeâ€Dimensional Superâ€Branched PdCu Nanoarchitectures Exposed on Controlled Crystal Facets. Chemistry - A European Journal, 2017, 23, 51-56.	3.3	24
79	A Simple Silver Nanowire Patterning Method Based on Poly(Ethylene Glycol) Photolithography and Its Application for Soft Electronics. Scientific Reports, 2017, 7, 2282.	3.3	55
80	Nanoarchitecture of MOF-derived nanoporous functional composites for hybrid supercapacitors. Journal of Materials Chemistry A, 2017, 5, 15065-15072.	10.3	146
81	Synthesis of Carbon Nanospheres Through Carbonization of <i>Areca nut</i> . Journal of Nanoscience and Nanotechnology, 2017, 17, 2837-2842.	0.9	16
82	Facile synthesis of nanoporous Li <sub>1+x</sub> V <sub>1â^'x</sub> O <sub>2</sub> @C composites as promising anode materials for lithium-ion batteries. Physical Chemistry Chemical Physics, 2017, 19, 9156-9163.	2.8	2
83	A Threeâ€Dimensionally Structured Electrocatalyst: Cobaltâ€Embedded Nitrogenâ€Doped Carbon Nanotubes/Nitrogenâ€Doped Reduced Graphene Oxide Hybrid for Efficient Oxygen Reduction. Chemistry - A European Journal, 2017, 23, 637-643.	3.3	50
84	Fabrication, Transport Current Testing, and Finite Element Analysis of MgB2 Racetrack Coils. Journal of Superconductivity and Novel Magnetism, 2017, 30, 2957-2962.	1.8	2
85	Redox-Active Polymers for Energy Storage Nanoarchitectonics. Joule, 2017, 1, 739-768.	24.0	400
86	Aggregated mesoporous nanoparticles for high surface area light scattering layer TiO2 photoanodes in Dye-sensitized Solar Cells. Scientific Reports, 2017, 7, 10341.	3.3	35
87	Preface for Special Topic: Nanogenerators. APL Materials, 2017, 5, .	5.1	10
88	Ni–Co Binary Hydroxide Nanotubes with Threeâ€Dimensionally Structured Nanoflakes: Synthesis and Application as Cathode Materials for Hybrid Supercapacitors. Chemistry - A European Journal, 2017, 23, 10133-10138.	3.3	4
89	Preferential growth of boron layer in magnesium diboride (MgB2) by Mg diffusion method. Journal of Alloys and Compounds, 2017, 725, 526-535.	5.5	12
90	Prussian Blue-Derived Synthesis of Hollow Porous Iron Pyrite Nanoparticles as Platinum-Free Counter Electrodes for Highly Efficient Dye-Sensitized Solar Cells. Chemistry - A European Journal, 2017, 23, 13263-13263.	3.3	0

#	Article	IF	CITATIONS
91	Highly Efficient Thin-Film Transistor via Cross-Linking of 1T Edge Functional 2H Molybdenum Disulfides. ACS Nano, 2017, 11, 12832-12839.	14.6	19
92	Prussian Blueâ€Derived Synthesis of Hollow Porous Iron Pyrite Nanoparticles as Platinumâ€Free Counter Electrodes for Highly Efficient Dyeâ€Sensitized Solar Cells. Chemistry - A European Journal, 2017, 23, 13284-13288.	3.3	25
93	Controlled growth of polythiophene nanofibers in TiO <sub>2</sub> nanotube arrays for supercapacitor applications. Journal of Materials Chemistry A, 2017, 5, 172-180.	10.3	76
94	Template Free Preparation of Heteroatoms Doped Carbon Spheres with Trace Fe for Efficient Oxygen Reduction Reaction and Supercapacitor. Advanced Energy Materials, 2017, 7, 1602002.	19.5	160
95	Doping-Induced Isotopic Mg11B2 Bulk Superconductor for Fusion Application. Energies, 2017, 10, 409.	3.1	7
96	Superior Electrocatalytic Activity of a Robust Carbonâ€Felt Electrode with Oxygenâ€Rich Phosphate Groups for Allâ€Vanadium Redox Flow Batteries. ChemSusChem, 2016, 9, 1329-1338.	6.8	95
97	Nanoarchitectures for Mesoporous Metals. Advanced Materials, 2016, 28, 993-1010.	21.0	357
98	Fly compound-eye inspired inorganic nanostructures with extraordinary visible-light responses. Materials Today Chemistry, 2016, 1-2, 84-89.	3.5	22
99	Strategic synthesis of mesoporous Pt-on-Pd bimetallic spheres templated from a polymeric micelle assembly. Journal of Materials Chemistry A, 2016, 4, 9169-9176.	10.3	32
100	All-in-one energy harvesting and storage devices. Journal of Materials Chemistry A, 2016, 4, 7983-7999.	10.3	245
101	Cyanoâ€Bridged Trimetallic Coordination Polymer Nanoparticles and Their Thermal Decomposition into Nanoporous Spinel Ferromagnetic Oxides. Chemistry - A European Journal, 2016, 22, 15042-15048.	3.3	10
102	Absorption dichroism of monolayer 1T′-MoTe <sub>2</sub> in visible range. 2D Materials, 2016, 3, 031010.	4.4	32
103	Graphene-like holey Co3O4 nanosheets as a highly efficient catalyst for oxygen evolution reaction. Nano Energy, 2016, 30, 267-275.	16.0	179
104	Evaluation of persistent-mode operation in a superconducting MgB <sub>2</sub> coil in solid nitrogen. Superconductor Science and Technology, 2016, 29, 04LT02.	3.5	24
105	CNTs grown on nanoporous carbon from zeolitic imidazolate frameworks for supercapacitors. Chemical Communications, 2016, 52, 13016-13019.	4.1	109
106	Electrochemical Property of Mesoporous Crystalline Iron Phosphonate Anode in Li-Ion Rechargeable Battery. Journal of Nanoscience and Nanotechnology, 2016, 16, 9180-9185.	0.9	5
107	Si/SiO <sub><i>x</i></sub> â€Conductive Polymer Coreâ€Shell Nanospheres with an Improved Conducting Path Preservation for Lithiumâ€Ion Battery. ChemSusChem, 2016, 9, 2754-2758.	6.8	42
108	Conductive polymers for next-generation energy storage systems: recent progress and new functions. Materials Horizons, 2016, 3, 517-535.	12.2	272

#	Article	IF	CITATIONS
109	First Synthesis of Continuous Mesoporous Copper Films with Uniformly Sized Pores by Electrochemical Soft Templating. Angewandte Chemie - International Edition, 2016, 55, 12746-12750.	13.8	50
110	First Synthesis of Continuous Mesoporous Copper Films with Uniformly Sized Pores by Electrochemical Soft Templating. Angewandte Chemie, 2016, 128, 12938-12942.	2.0	15
111	Interface miscibility induced double-capillary carbon nanofibers for flexible electric double layer capacitors. Nano Energy, 2016, 28, 232-240.	16.0	67
112	Rechargeable lithium–air batteries: a perspective on the development of oxygen electrodes. Journal of Materials Chemistry A, 2016, 4, 14050-14068.	10.3	155
113	Nanoarchitectures for Metal–Organic Framework-Derived Nanoporous Carbons toward Supercapacitor Applications. Accounts of Chemical Research, 2016, 49, 2796-2806.	15.6	670
114	A Facile Approach for Constructing Conductive Polymer Patterns for Application in Electrochromic Devices and Flexible Microelectrodes. ACS Applied Materials & Interfaces, 2016, 8, 33175-33182.	8.0	40
115	Zeolitic imidazolate framework (ZIF-8) derived nanoporous carbon: the effect of carbonization temperature on the supercapacitor performance in an aqueous electrolyte. Physical Chemistry Chemical Physics, 2016, 18, 29308-29315.	2.8	213
116	A new approach to a superconducting joining process for carbon-doped MgB <sub>2</sub> conductor. Superconductor Science and Technology, 2016, 29, 095001.	3.5	19
117	Tunableâ€Sized Polymeric Micelles and Their Assembly for the Preparation of Large Mesoporous Platinum Nanoparticles. Angewandte Chemie, 2016, 128, 10191-10195.	2.0	14
118	Tunableâ€ <b>s</b> ized Polymeric Micelles and Their Assembly for the Preparation of Large Mesoporous Platinum Nanoparticles. Angewandte Chemie - International Edition, 2016, 55, 10037-10041.	13.8	122
119	Deliberate Design of TiO <sub>2</sub> Nanostructures towards Superior Photovoltaic Cells. Chemistry - A European Journal, 2016, 22, 11357-11364.	3.3	25
120	Formation of mesopores inside platinum nanospheres by using double hydrophilic block copolymers. Materials Letters, 2016, 182, 190-193.	2.6	5
121	Bimetallic Metal-Organic Frameworks for Controlled Catalytic Graphitization of Nanoporous Carbons. Scientific Reports, 2016, 6, 30295.	3.3	314
122	Unique nanocrystalline frameworks in mesoporous tin phosphate prepared through a hydrofluoric acid assisted chemical reaction. Journal of Materials Chemistry A, 2016, 4, 18091-18099.	10.3	14
123	Improvement in the transport critical current density and microstructure of isotopic Mg11B2 monofilament wires by optimizing the sintering temperature. Scientific Reports, 2016, 6, 36660.	3.3	7
124	Synthesis of Cobalt Sulfide/Sulfur Doped Carbon Nanocomposites with Efficient Catalytic Activity in the Oxygen Evolution Reaction. Chemistry - A European Journal, 2016, 22, 18259-18264.	3.3	43
125	Ultrahigh performance supercapacitors utilizing core–shell nanoarchitectures from a metal–organic framework-derived nanoporous carbon and a conducting polymer. Chemical Science, 2016, 7, 5704-5713.	7.4	236
126	Electrospun Polyacrylonitrile–Ionic Liquid Nanofibers for Superior PM <sub>2.5</sub> Capture Capacity. ACS Applied Materials & Interfaces, 2016, 8, 7030-7036.	8.0	92

#	Article	IF	CITATIONS
127	Directional dependent piezoelectric effect in CVD grown monolayer MoS 2 for flexible piezoelectric nanogenerators. Nano Energy, 2016, 22, 483-489.	16.0	197
128	Controlled delivery of drugs adsorbed onto porous Fe 3 O 4 structures by application of AC/DC magnetic fields. Microporous and Mesoporous Materials, 2016, 226, 243-250.	4.4	27
129	The smallest quaternary ammonium salts with ether groups for high-performance electrochemical double layer capacitors. Chemical Science, 2016, 7, 1791-1796.	7.4	45
130	Magnesium diboride(MgB <sub>2</sub> ) wires for applications. Progress in Superconductivity and Cryogenics (PSAC), 2016, 18, 1-5.	0.3	2
131	Controlled Synthesis of Nanoporous Nickel Oxide with Twoâ€Dimensional Shapes through Thermal Decomposition of Metal–Cyanide Hybrid Coordination Polymers. Chemistry - A European Journal, 2015, 21, 3509-3509.	3.3	2
132	Polymeric Micelle Assembly for the Smart Synthesis of Mesoporous Platinum Nanospheres with Tunable Pore Sizes. Angewandte Chemie - International Edition, 2015, 54, 11073-11077.	13.8	160
133	Electrochemical Synthesis of Mesoporous Pt Nanowires with Highly Electrocatalytic Activity toward Methanol Oxidation Reaction. Electrochimica Acta, 2015, 183, 107-111.	5.2	22
134	Fish-scale bio-inspired multifunctional ZnO nanostructures. NPG Asia Materials, 2015, 7, e232-e232.	7.9	56
135	MgB <sub>2</sub> superconducting joints for persistent current operation. Superconductor Science and Technology, 2015, 28, 065017.	3.5	18
136	Cover Picture: Controlled Synthesis of Nanoporous Nickel Oxide with Twoâ€Đimensional Shapes through Thermal Decomposition of Metal–Cyanide Hybrid Coordination Polymers (Chem. Eur. J.) Tj ETQq0 0 0	rg <b>B1</b> 3/Ove	rlo <b>o</b> k 10 Tf 5(
137	N719- and D149-sensitized 3D hierarchical rutile TiO <sub>2</sub> solar cells—a comparative study. Physical Chemistry Chemical Physics, 2015, 17, 7208-7213.	2.8	21
138	The effect of surface passivation on the structure of sulphur-rich PbS colloidal quantum dots for photovoltaic application. Nanoscale, 2015, 7, 5706-5711.	5.6	39
139	Nanopatterned Textile-Based Wearable Triboelectric Nanogenerator. ACS Nano, 2015, 9, 3501-3509.	14.6	612
140	Mesoporous Iron Phosphonate Electrodes with Crystalline Frameworks for Lithium-Ion Batteries. Chemistry of Materials, 2015, 27, 1082-1089.	6.7	138
141	Facile potentiostatic preparation of functionalized polyterthiophene-anchored graphene oxide as a metal-free electrocatalyst for the oxygen reduction reaction. Journal of Materials Chemistry A, 2015, 3, 5426-5433.	10.3	35
142	A Bi-layer TiO <sub>2</sub> photoanode for highly durable, flexible dye-sensitized solar cells. Journal of Materials Chemistry A, 2015, 3, 4679-4686.	10.3	27
143	Controlled Synthesis of Nanoporous Nickel Oxide with Twoâ€Dimensional Shapes through Thermal Decomposition of Metal–Cyanide Hybrid Coordination Polymers. Chemistry - A European Journal, 2015, 21, 3605-3612.	3.3	64
144	A Highly Resilient Mesoporous SiO <sub><i>x</i></sub> Lithium Storage Material Engineered by Oil–Water Templating. ChemSusChem, 2015, 8, 688-694.	6.8	45

#	Article	IF	CITATIONS
145	One-dimensional manganese-cobalt oxide nanofibres as bi-functional cathode catalysts for rechargeable metal-air batteries. Scientific Reports, 2015, 5, 7665.	3.3	86
146	Magnetic nanoparticles for "smart liposomes― European Biophysics Journal, 2015, 44, 647-654.	2.2	23
147	Phase patterning for ohmic homojunction contact in MoTe <sub>2</sub> . Science, 2015, 349, 625-628.	12.6	918
148	Shape-controlled synthesis of mesoporous iron phosphate materials with crystallized frameworks. Chemical Communications, 2015, 51, 13806-13809.	4.1	20
149	A technology review of electrodes and reaction mechanisms in vanadium redox flow batteries. Journal of Materials Chemistry A, 2015, 3, 16913-16933.	10.3	565
150	Carbon doping induced imperfections on MgB2 superconducting wire. Journal of Analytical Science and Technology, 2015, 6, .	2.1	20
151	Control of core structure in MgB2 wire through tailoring boron powder. Journal of Alloys and Compounds, 2015, 636, 29-33.	5.5	12
152	Correlation between in-field Jc enhancement and grain connectivity in co-doped MgB2 superconductor. Materials Letters, 2015, 139, 333-335.	2.6	16
153	Asymmetric Supercapacitors Using 3D Nanoporous Carbon and Cobalt Oxide Electrodes Synthesized from a Single Metal–Organic Framework. ACS Nano, 2015, 9, 6288-6296.	14.6	890
154	Rational design of coaxial structured carbon nanotube–manganese oxide (CNT–MnO <sub>2</sub> ) for energy storage application. Nanotechnology, 2015, 26, 204004.	2.6	55
155	Fabrication of Asymmetric Supercapacitors Based on Coordination Polymer Derived Nanoporous Materials. Electrochimica Acta, 2015, 183, 94-99.	5.2	24
156	Bandgap opening in few-layered monoclinic MoTe2. Nature Physics, 2015, 11, 482-486.	16.7	800
157	Two-step self-assembly of hierarchically-ordered nanostructures. Journal of Materials Chemistry A, 2015, 3, 11688-11699.	10.3	51
158	A Facile Preparation of Mesoporous Carbon Composites with Well-Dispersed Pd Nanoparticles and Their Utilization as Supports for Pt Catalysts. Electrochimica Acta, 2015, 183, 112-118.	5.2	7
159	Significantly enhanced critical current density in nano-MgB <sub>2</sub> grains rapidly formed at low temperature with homogeneous carbon doping. Superconductor Science and Technology, 2015, 28, 055005.	3.5	21
160	Surfaceâ€Tunable Bioluminescence Resonance Energy Transfer via Geometryâ€Controlled ZnO Nanorod Coordination. Small, 2015, 11, 3469-3475.	10.0	4
161	Electrospun manganese–cobalt oxide hollow nanofibres synthesized via combustion reactions and their lithium storage performance. Nanoscale, 2015, 7, 8351-8355.	5.6	111
162	Incorporation of conductive polymer into soft carbon electrodes for lithium ion capacitors. Journal of Power Sources, 2015, 299, 49-56.	7.8	26

#	Article	IF	CITATIONS
163	Improved transport critical current properties in glycerin-doped MgB2 wire using milled boron powder and a solid-state reaction of 600°C. Journal of Alloys and Compounds, 2015, 650, 794-798.	5.5	14
164	Surfactant-Directed Synthesis of Mesoporous Pd Films with Perpendicular Mesochannels as Efficient Electrocatalysts. Journal of the American Chemical Society, 2015, 137, 11558-11561.	13.7	100
165	Trap-Assisted Transport and Non-Uniform Charge Distribution in Sulfur-Rich PbS Colloidal Quantum Dot-based Solar Cells with Selective Contacts. ACS Applied Materials & Interfaces, 2015, 7, 26455-26460.	8.0	9
166	Porous nanoarchitectures of spinel-type transition metal oxides for electrochemical energy storage systems. Physical Chemistry Chemical Physics, 2015, 17, 30963-30977.	2.8	142
167	Mesoporous Hierarchical Anatase for Dye-sensitized Solar Cells Achieving Over 10% Conversion Efficiency. Electrochimica Acta, 2015, 153, 393-398.	5.2	28
168	Ultra-High Performance, High-Temperature Superconducting Wires via Cost-effective, Scalable, Co-evaporation Process. Scientific Reports, 2015, 4, 4744.	3.3	42
169	Large-scale synthesis of coaxial carbon nanotube/Ni(OH)2 composites for asymmetric supercapacitor application. Nano Energy, 2015, 11, 211-218.	16.0	439
170	Mesoporous anatase single crystals for efficient Co(2+/3+)-based dye-sensitized solar cells. Nano Energy, 2015, 11, 557-567.	16.0	54
171	The formation of nano-layered grains and their enhanced superconducting transition temperature in Mg-doped FeSe0.9 bulks. Scientific Reports, 2015, 4, 6481.	3.3	9
172	Towards Vaporized Molecular Discrimination: A Quartz Crystal Microbalance (QCM) Sensor System Using Cobalt ontaining Mesoporous Graphitic Carbon. Chemistry - an Asian Journal, 2014, 9, 3238-3244.	3.3	33
173	Scalable Integration of Li <sub>5</sub> FeO <sub>4</sub> towards Robust, Highâ€Performance Lithiumâ€Ion Hybrid Capacitors. ChemSusChem, 2014, 7, 3138-3144.	6.8	63
174	Characterization of Superconducting BSCCO/CaSiO <sub>3</sub> and BSCCO/CaZrO <sub>3</sub> Ag PIT Wires. Advanced Materials Research, 2014, 975, 106-110.	0.3	0
175	Enhancement of transition temperature in Fe <i>x</i> Se0.5Te0.5 film via iron vacancies. Applied Physics Letters, 2014, 104, .	3.3	31
176	Microstructural and crystallographic imperfections of MgB2 superconducting wire and their correlation with the critical current density. AIP Advances, 2014, 4, .	1.3	8
177	Channelled Porous TiO <sub>2</sub> Synthesized with a Waterâ€inâ€Oil Microemulsion. Chemistry - A European Journal, 2014, 20, 10451-10455.	3.3	6
178	Surface Chemistry: Bio-Inspired Multifunctional Metallic Foams Through the Fusion of Different Biological Solutions (Adv. Funct. Mater. 18/2014). Advanced Functional Materials, 2014, 24, 2720-2720.	14.9	0
179	Zr <sup>4+</sup> Doping in Li <sub>4</sub> Ti <sub>5</sub> O <sub>12</sub> Anode for Lithiumâ€lon Batteries: Open Li <sup>+</sup> Diffusion Paths through Structural Imperfection. ChemSusChem, 2014, 7, 1451-1457.	6.8	92
180	Bioâ€Inspired Multifunctional Metallic Foams Through the Fusion of Different Biological Solutions. Advanced Functional Materials, 2014, 24, 2721-2726.	14.9	46

#	Article	IF	CITATIONS
181	Fabrication of symmetric supercapacitors based on MOF-derived nanoporous carbons. Journal of Materials Chemistry A, 2014, 2, 19848-19854.	10.3	419
182	Highly connected hierarchical textured TiO <sub>2</sub> spheres as photoanodes for dye-sensitized solar cells. Journal of Materials Chemistry A, 2014, 2, 8902-8909.	10.3	57
183	Percolative nature of current transport in polycrystalline MgB2 wires. Solid State Communications, 2014, 181, 20-23.	1.9	5
184	Power-Law Relationship Between Critical Current Density, Microstructure, and the n-Value in MgB2 Superconductor Wires. Journal of Superconductivity and Novel Magnetism, 2014, 27, 1643-1645.	1.8	7
185	Direct Growth of Cobalt Hydroxide Rods on Nickel Foam and Its Application for Energy Storage. Chemistry - A European Journal, 2014, 20, 3084-3088.	3.3	127
186	Flyâ€Eye Inspired Superhydrophobic Antiâ€Fogging Inorganic Nanostructures. Small, 2014, 10, 3001-3006.	10.0	290
187	Generalized self-assembly of scalable two-dimensional transition metal oxide nanosheets. Nature Communications, 2014, 5, 3813.	12.8	741
188	Hydrogen Silsequioxane-Derived Si/SiO <sub><i>x</i></sub> Nanospheres for High-Capacity Lithium Storage Materials. ACS Applied Materials & Interfaces, 2014, 6, 9608-9613.	8.0	93
189	Synthesis of Mesoporous TiO <sub>2</sub> /SiO <sub>2</sub> Hybrid Films as an Efficient Photocatalyst by Polymeric Micelle Assembly. Chemistry - A European Journal, 2014, 20, 6027-6032.	3.3	123
190	Chiral Recognition of Proline Enantiomers by the Catalytic Oxygen Reduction and Formation of Cu(II)â€Polymer Complex Crystals. Electroanalysis, 2014, 26, 2110-2117.	2.9	2
191	A case study on fibrous porous SnO 2 anode for robust, high-capacity lithium-ion batteries. Nano Energy, 2014, 10, 53-62.	16.0	179
192	Superhydrophobic Materials: Fly-Eye Inspired Superhydrophobic Anti-Fogging Inorganic Nanostructures (Small 15/2014). Small, 2014, 10, 3000-3000.	10.0	3
193	Sn <sub>4+<i>x</i></sub> P <sub>3</sub> @ Amorphous Snâ€P Composites as Anodes for Sodiumâ€lon Batteries with Low Cost, High Capacity, Long Life, and Superior Rate Capability. Advanced Materials, 2014, 26, 4037-4042.	21.0	298
194	Multiwalled carbon nanotube-derived superior electrical, mechanical and thermal properties in MgB2 wires. Scripta Materialia, 2014, 88, 13-16.	5.2	30
195	Ultrafine SnO <sub>2</sub> nanoparticle loading onto reduced graphene oxide as anodes for sodium-ion batteries with superior rate and cycling performances. Journal of Materials Chemistry A, 2014, 2, 529-534.	10.3	297
196	Core–Shell Structured Silicon Nanoparticles@TiO <sub>2–<i>x</i></sub> /Carbon Mesoporous Microfiber Composite as a Safe and High-Performance Lithium-Ion Battery Anode. ACS Nano, 2014, 8, 2977-2985.	14.6	227
197	Rational design of MgB2 conductors toward practical applications. Cryogenics, 2014, 63, 160-165.	1.7	49
198	A new strategy for integrating abundant oxygen functional groups into carbon felt electrode for vanadium redox flow batteries. Scientific Reports, 2014, 4, 6906.	3.3	136

#	Article	IF	CITATIONS
199	3D Hierarchical Rutile TiO2 and Metal-free Organic Sensitizer Producing Dye-sensitized Solar Cells 8.6% Conversion Efficiency. Scientific Reports, 2014, 4, 5769.	3.3	142
200	Robust superhydrophobicity of hierarchical ZnO hollow microspheres fabricated by two-step self-assembly. Nano Research, 2013, 6, 726-735.	10.4	60
201	Controlled Ag-driven superior rate-capability of Li4Ti5O12 anodes for lithium rechargeable batteries. Nano Research, 2013, 6, 365-372.	10.4	75
202	Aqueous Colloidal Stability Evaluated by Zeta Potential Measurement and Resultant <scp><scp>TiO</scp></scp> <sub>2</sub> for Superior Photovoltaic Performance. Journal of the American Ceramic Society, 2013, 96, 2636-2643.	3.8	26
203	Synergetic Combination of LIMD With CHPD for the Production of Economical and High Performance \$hbox{MgB}_{2}\$ Wires. IEEE Transactions on Applied Superconductivity, 2013, 23, 6200704-6200704.	1.7	11
204	Architecture designed ZnO hollow microspheres with wide-range visible-light photoresponses. Journal of Materials Chemistry C, 2013, 1, 6924.	5.5	29
205	Morphology-controllable 1D–3D nanostructured TiO2bilayer photoanodes for dye-sensitized solar cells. Chemical Communications, 2013, 49, 966-968.	4.1	94
206	Nanocomposites of silicon and carbon derived from coal tar pitch: Cheap anode materials for lithium-ion batteries with long cycle life and enhanced capacity. Electrochimica Acta, 2013, 93, 213-221.	5.2	93
207	Structurally and Electronically Designed TiO <sub>2</sub> N <sub><i>x</i></sub> Nanofibers for Lithium Rechargeable Batteries. ACS Applied Materials & Interfaces, 2013, 5, 691-696.	8.0	63
208	Magnetization Loss of MgB2 Superconducting Wire at Various Temperatures. Journal of Superconductivity and Novel Magnetism, 2013, 26, 1531-1535.	1.8	1
209	Li <sub>2</sub> RuO <sub>3</sub> as an Additive for High-Energy Lithium-Ion Capacitors. Journal of Physical Chemistry C, 2013, 117, 11471-11478.	3.1	55
210	Structurally stabilized mesoporous TiO2 nanofibres for efficient dye-sensitized solar cells. APL Materials, 2013, 1, .	5.1	22
211	Magnetotransport dependence on the field magnitude and direction in large area epitaxial graphene film on stretchable substrates. Applied Physics Letters, 2013, 102, .	3.3	4
212	Enhancing the Superconducting Properties of Magnesium Diboride Without Doping. Journal of the American Ceramic Society, 2013, 96, 2893-2897.	3.8	5
213	Prediction of AC Losses in \$hbox{MgB}_{2}\$ Superconducting Wires as a Function of Transport Currents and Temperatures. IEEE Transactions on Applied Superconductivity, 2012, 22, 6200404-6200404.	1.7	1
214	Superior MgB\$_{2}\$ Superconducting Wire Performance through Oxygen-Free Pyrene Additive. Applied Physics Express, 2012, 5, 013101.	2.4	7
215	The Effects of Graphene Doping on the In-Field <i>J<sub>c</sub></i> of MgB <sub>2</sub> Wires. Journal of Nanoscience and Nanotechnology, 2012, 12, 1402-1405.	0.9	6
216	Microscopic role of carbon on MgB2 wire for critical current density comparable to NbTi. NPG Asia Materials, 2012, 4, e3-e3.	7.9	120

#	Article	IF	CITATIONS
217	Effect of frozen spin on the magnetocaloric property of La0.7Ca0.3CoO3 polycrystalline and single crystal samples. Journal of Alloys and Compounds, 2012, 510, 125-133.	5.5	22
218	Continually adjustable oriented 1D TiO2 nanostructure arrays with controlled growth of morphology and their application in dye-sensitized solar cells. CrystEngComm, 2012, 14, 5472.	2.6	32
219	Structural control of d-f interaction in the CeFe <sub>1â^x</sub> Ru <sub>x</sub> AsO system. Europhysics Letters, 2012, 99, 57009.	2.0	8
220	Improved photovoltaic performance of dye-sensitized solar cells with modified self-assembling highly ordered mesoporous TiO2 photoanodes. Journal of Materials Chemistry, 2012, 22, 11711.	6.7	37
221	Anisotropic and excellent magnetocaloric properties of La0.7Ca0.3MnO3 single crystal with anomalous magnetization. Materials Science and Engineering B: Solid-State Materials for Advanced Technology, 2012, 177, 48-53.	3.5	15
222	AC Loss in MgB\$_{2}\$ Superconducting Wires at Various Operating Temperatures. IEEE Transactions on Applied Superconductivity, 2011, 21, 3342-3346.	1.7	6
223	Large magnetic entropy change near room temperature in La0.7(Ca0.27Ag0.03)MnO3 perovskite. Journal of Alloys and Compounds, 2011, 509, 3699-3704.	5.5	37
224	Rational Design of 3D Dendritic TiO <sub>2</sub> Nanostructures with Favorable Architectures. Journal of the American Chemical Society, 2011, 133, 19314-19317.	13.7	387
225	Structurally stabilized olivine lithium phosphate cathodes with enhanced electrochemical properties through Fe doping. Energy and Environmental Science, 2011, 4, 4978.	30.8	59
226	Tailored Materials for Highâ€Performance MgB <sub>2</sub> Wire. Advanced Materials, 2011, 23, 4942-4946.	21.0	76
227	Nanoengineered Superconducting Wire: Tailored Materials for Highâ€Performance MgB <sub>2</sub> Wire (Adv. Mater. 42/2011). Advanced Materials, 2011, 23, 4820-4820.	21.0	0
228	Improvement of refrigerant capacity of La0.7Ca0.3MnO3 material with a few percent Co doping. Journal of Magnetism and Magnetic Materials, 2011, 323, 138-143.	2.3	25
229	Correlation between critical current density and n-value in MgB2/Nb/Monel superconductor wires. Physica C: Superconductivity and Its Applications, 2010, 470, 1207-1210.	1.2	31
230	The effects of C substitution and disorder on the field dependent critical current density in MgB2 with nano-SiC additions. Physica C: Superconductivity and Its Applications, 2010, 470, 1211-1215.	1.2	2
231	Influence of hot-pressing on MgB2/Nb/Monel wires. Physica C: Superconductivity and Its Applications, 2010, 470, 1426-1429.	1.2	12
232	Superconducting Properties of \${m MgB}_{2}\$ Wire Using Ball-Milled Low Purity Boron. IEEE Transactions on Applied Superconductivity, 2009, 19, 2714-2717.	1.7	0
233	Determination of the relative influences of carbon doping and disorder on field and temperature dependent critical current density of MgB <sub>2</sub> . Superconductor Science and Technology, 2009, 22, 125005.	3.5	8
234	Lattice Parameter, Lattice Disorder and Resistivity of Carbohydrate Doped MgB2 and Their Correlation with the Transition Temperature. Journal of Nanoscience and Nanotechnology, 2009, 9, 7477-80.	0.9	4

#	Article	IF	CITATIONS
235	Stress/Strain Induced Flux Pinning in Highly Dense \${m MgB}_{2}\$ Bulks. IEEE Transactions on Applied Superconductivity, 2009, 19, 2722-2725.	1.7	6
236	YBCO Film With Sm Addition Using Low-Fluorine TFA-MOD Approach. IEEE Transactions on Applied Superconductivity, 2009, 19, 3208-3211.	1.7	9
237	Development of Textured Au Layer on Ni Substrate for YBCO Coated Conductors. IEEE Transactions on Applied Superconductivity, 2005, 15, 2675-2678.	1.7	0
238	Magnetization Loss of Stacked Bi-2223/Ag Tapes in External Magnetic Field. IEEE Transactions on Applied Superconductivity, 2005, 15, 1607-1610.	1.7	4
239	Effect of W Addition on the Microstructure and Properties of Ni-W Substrates for Coated Conductors. IEEE Transactions on Applied Superconductivity, 2005, 15, 2683-2686.	1.7	8
240	Fabrication and Characteristics of the Joint Properties in <tex>\$(hboxBi,hboxPb)_2hboxSr_2hboxCa_2hboxCu_3hboxO_rm x\$</tex> Closed Double Pancake Coil. IEEE Transactions on Applied Superconductivity, 2004, 14, 1094-1097.	1.7	5
241	AC Transport Current Loss of Horizontally Attached Bi-2223/Ag Tapes. IEEE Transactions on Applied Superconductivity, 2004, 14, 1894-1897.	1.7	18
242	Development of Textured Ni Substrates for Coated Conductor Prepared by Powder Metallurgy and Plasma Arc Melting Method. IEEE Transactions on Applied Superconductivity, 2004, 14, 1086-1089.	1.7	5
243	Development and characteristics of persistent mode in HTS magnet. Physica C: Superconductivity and Its Applications, 2004, 412-414, 1026-1029.	1.2	6
244	Design, fabrication and testing of superconducting dc reactor for 1.2 kV/80 a inductive fault current limiter. IEEE Transactions on Applied Superconductivity, 2003, 13, 2008-2011.	1.7	12
245	Characterization of thermal conductivity and mechanical properties of Ag-alloy sheathed Bi(Pb)-Sr-Ca-Cu-O superconductor tape. IEEE Transactions on Applied Superconductivity, 2003, 13, 2956-2959.	1.7	7
246	Superconducting joint of multifilamentary Bi(Pb)-Sr-Ca-Cu-O tapes. IEEE Transactions on Applied Superconductivity, 2003, 13, 2996-2999.	1.7	2
247	Measurement of joint properties of Bi(pb)-Sr-Ca-Cu-O (2223) tapes by field decay technique. IEEE Transactions on Applied Superconductivity, 2003, 13, 2992-2995.	1.7	10
248	A superconducting joint between BiÂPbÂSrÂCaÂCuÂO multifilamentary tapes. Superconductor Science and Technology, 2002, 15, 1600-1605.	3.5	14
249	A study on joining method of Bi–Pb–Sr–Ca–Cu–O multifilamentary tape. Physica C: Superconductivity and Its Applications, 2002, 372-376, 909-912.	1.2	15
250	Critical current degradation in jointed area of Ag-sheathed BSCCO tapes. IEEE Transactions on Applied Superconductivity, 2001, 11, 3014-3017.	1.7	0
251	Superconducting joint between Bi-Pb-Sr-Ca-Cu-O superconductor tapes. IEEE Transactions on Applied Superconductivity, 2000, 10, 1182-1185.	1.7	9
252	Ultrathin Noncontact-Mode Triboelectric Nanogenerator Triggered by Giant Dielectric Material Adaption. ACS Energy Letters, 0, , 1189-1197.	17.4	40